Indonesian Journal of Chemical Research

http://ojs3.unpatti.ac.id/index.php/ijcr

Indo. J. Chem. Res., 13 (2), 186-196, 2025

From Zircon Sand to Advanced Functional Materials: Synthesis and Characterization of Zirconium-Based Metal Organic Frameworks

Berryl Vendo Palapessy, Brilyan Muhammad Rasyid Reda, Fainan Failamani, Aep Patah*

Inorganic & Physical Chemistry Research Division, Institut Teknologi Bandung, Jl. Ganesha 10, Bandung, 40132, Indonesia *Corresponding Author: aep@itb.ac.id

Received: June 2025

Received in revised: August 2025 Accepted: September 2025 Available online: September 2025

Abstract

This study presents an integrated approach for converting zircon sand into functional materials based on zirconium metal–organic frameworks (Zr-MOFs). Zirconium was extracted through three main steps: alkali fusion, water leaching, and nitric acid leaching, resulting in a precursor identified as Zr(OH)₂(NO₃)₂·1.33H₂O (ZON). Characterization using XRF, FTIR, XRD, and SEM-EDX revealed that ZON possesses a high zirconium content (94.87% relative to the total metal content) and distinct structural features. The ZON compound was subsequently utilized as a novel precursor in synthesizing of three types of Zr-MOFs: UiO-66, MOFs-801, and MOFs-808. Structural and morphological analyses indicated that all three MOFs were successfully formed with high crystallinity. These findings demonstrate that locally sourced zircon sand has strong potential as a sustainable and cost-effective raw material for MOF synthesis, while also bridging the knowledge gap between zirconium extraction and the development of sustainable materials chemistry based on local mineral resources.

Keywords: Zircon sand, zirconium extraction, local mineral utilization, metal—organic frameworks (MOFs), Zr-MOFs

INTRODUCTION

Zirconium is a transition metal naturally occurring in two primary mineral forms: zircon (ZrSiO₄) and baddeleyite (ZrO₂). Among these, zircon is the more abundant and is commonly found in association with igneous, metamorphic, and sedimentary rocks, as well as in heavy mineral deposits such as beach sands (Finch, 2003; Emsley, 2014). To obtain zircon in a concentrated and purified form, it must first be separated from associated gangue minerals via wet gravity separation, followed by magnetic and electrostatic methods (Tahli and Wahyudi, 2017; Sajima, et al. 2020). The extraction of Zr from zircon requires the disruption of the strong chemical bonds between ZrO₂ and SiO₂ within the zircon lattice (Da Silva, et al., 2012). This can be achieved through chemical treatment or high-temperature thermal processes, depending on the targeted efficiency and processing approach, with alkali fusion being one of the most commonly employed methods (Sun et al., 2019; Sun et al., 2024). Developing effective methods to isolate zirconium from natural sources is essential for its downstream applications in catalysts and advanced ceramic materials. Several studies have reported the utilization of zircon sand in the synthesis

of functional materials, including yttria-stabilized zirconia (Rahmawati, et al., 2016), ZrO2-TiO2 nanocomposites as photocatalysts for methylene blue degradation (Permadani, et al., 2016), polyaniline/ZrO₂ composites for anticorrosion coatings (Nadliriyah et al., 2019), and ZrO₂ catalyst for biodiesel production (Widayat, et al. 2024). One of the most rapidly growing classes of zirconium-based materials is metal-organic frameworks (Zr-MOFs), which are known for their high surface area, tunable porosity, and exceptional structural stability. Representative examples of Zr-MOFs, such as the UiO (Ru et al., 2021), MIP(Lv et al., 2022), and DUT series (Gutiérrez-Serpa et al., 2022) have been widely explored, typically synthesized using high-purity zirconium precursors such as ZrCl₄ or ZrOCl₂·8H₂O (Chattopadhyay et al. 2024; Su et al., 2024). However, reliance on commercial precursors presents challenges in terms of cost and sustainability, particularly for large-scale applications. Consequently, exploring of alternative zirconium sources that are more abundant and environmentally benign is crucial to support the development of sustainable materials technologies. Despite the high zirconium content in zircon sand, its direct utilization as a raw material for Zr-MOF synthesis remains limited. Most prior studies have

focused on the leaching and purification of zirconium from zircon (A. H. Ali, 2022; Ali, et. al., 2023), while integration of the extracted species into MOF frameworks is still rarely pursued. This indicates a significant knowledge gap, while simultaneously presenting an opportunity to develop zirconium-based MOFs from local mineral resources. This study aims to establish a transformation approach for converting zircon sand into Zr-MOF functional materials via zirconium extraction, solvothermal synthesis, and comprehensive characterization. Particular emphasis is placed on evaluating the structure and morphology of the synthesized materials to assess their viability as functional materials. Through this approach, the study seeks to contribute scientifically to valorizing of local mineral resources for developing of advanced, sustainable, and high-value materials.

METHODOLOGY

Materials and Instrumentals

Zircon sand (ZrSiO₄) was sourced from a local supplier in the Bandung area, originating from the Central Kalimantan region, Indonesia. The acquired sand had been cleaned through a magnetic separation process to remove black-colored impurities. Terephthalic acid (H₂BDC), fumaric acid (H₂Fum), trimesic acid (H₃BTC), dimethylformamide (DMF), glacial acetic acid (CH3COOH), and ethanol were procured commercially from Sigma-Aldrich and used without further purification. All washing procedures were conducted using high-purity demineralized water. The elemental composition of zircon sand and its leaching products was analyzed by X-ray fluorescence (Orbis Micro-XRF Analyzer). Functional groups were identified using Fourier Transform Infrared (FT-IR) spectroscopy (Shimadzu 470) 4000–400 cm⁻¹ range employing the KBr pellet technique. Structural characterization was conducted via powder X-ray diffraction (P-XRD) using a Rigaku MiniFlex diffractometer with Cu K α radiation (λ_1 = 1.540593 Å; $\lambda_2 = 1.544414$ Å). Particle morphology and surface features were examined using a scanning electron microscope (Thermo Scientific Phenom ProX G6 Desktop SEM).

Methods

1. Synthesis of ZON

A total of 20 g of zircon sand was mixed with 24 g of NaOH (mass ratio 1:1.2). The mixture was subjected to

alkali fusion at 700 °C for 3 h. The resulting white solid was washed several times with deionized water (solid-to-liquid ratio of 1:50) until the pH remained constant. The washed solid was subsequently dried at 105 °C. The extraction of zirconia was carried out by treating the dried solid with 10 M nitric acid (solid-to-liquid ratio of 1:50) under heating. The solution was evaporated until its volume was reduced by half and exhibited a yellowish color. The filtrate was cooled overnight in an ice bath to promote crystal nucleation. The solution was then concentrated by evaporation, yielding a white solid. This solid was carefully washed with deionized water and small portions of ethanol, then dried at 85 °C. The resulting product was designated as ZON.

2. Synthesis of UiO-66

UiO-66 was synthesized via a solvothermal method with slight modifications from previously reported procedures (Qiu et al. 2017). A mixture of 1.25 mmol H₂BDC and 1.25 mmol ZON was prepared in a solvent composed of 30 mL DMF and 14.13 mL glacial acetic acid. The mixture was ultrasonicated until a homogeneous solution formed. The resulting solution was then heated at 120 °C for 24 hours under solvothermal conditions. The obtained solid was washed multiple times with deionized water and ethanol, then dried at 60 °C overnight.

3. Synthesis of MOFs-801

MOF-801 was synthesized using a solvothermal approach with slight modifications to the procedure described by Ebrahim et al. (2024). Briefly, 1.25 mmol of H₂Fum and 1.25 mmol of ZON were dissolved in a solvent mixture of 5.04 mL of DMF and 1.77 mL of formic acid, followed by ultrasonication until a clear solution. The solution was then heated at 130 °C for 10 h under solvothermal conditions. The resulting solid was collected, thoroughly washed with DMF and ethanol, and dried at 60 °C overnight.

4. Synthesis of MOFs-808

MOF-808 was synthesized via a solvothermal method with minor modifications to previously reported procedures(Nguyen et al., 2021; Nguyen et al., 2023). A mixture of 0.4167 mmol H₃BTC and 1.25 mmol ZON was dissolved in a solvent mixture of 20 mL DMF and 20 mL formic acid by ultrasonication. The solution was then heated at 120 °C for 48 h under solvothermal conditions. The resulting precipitate was collected, washed thoroughly with DMF and ethanol, and dried at 70 °C overnight.

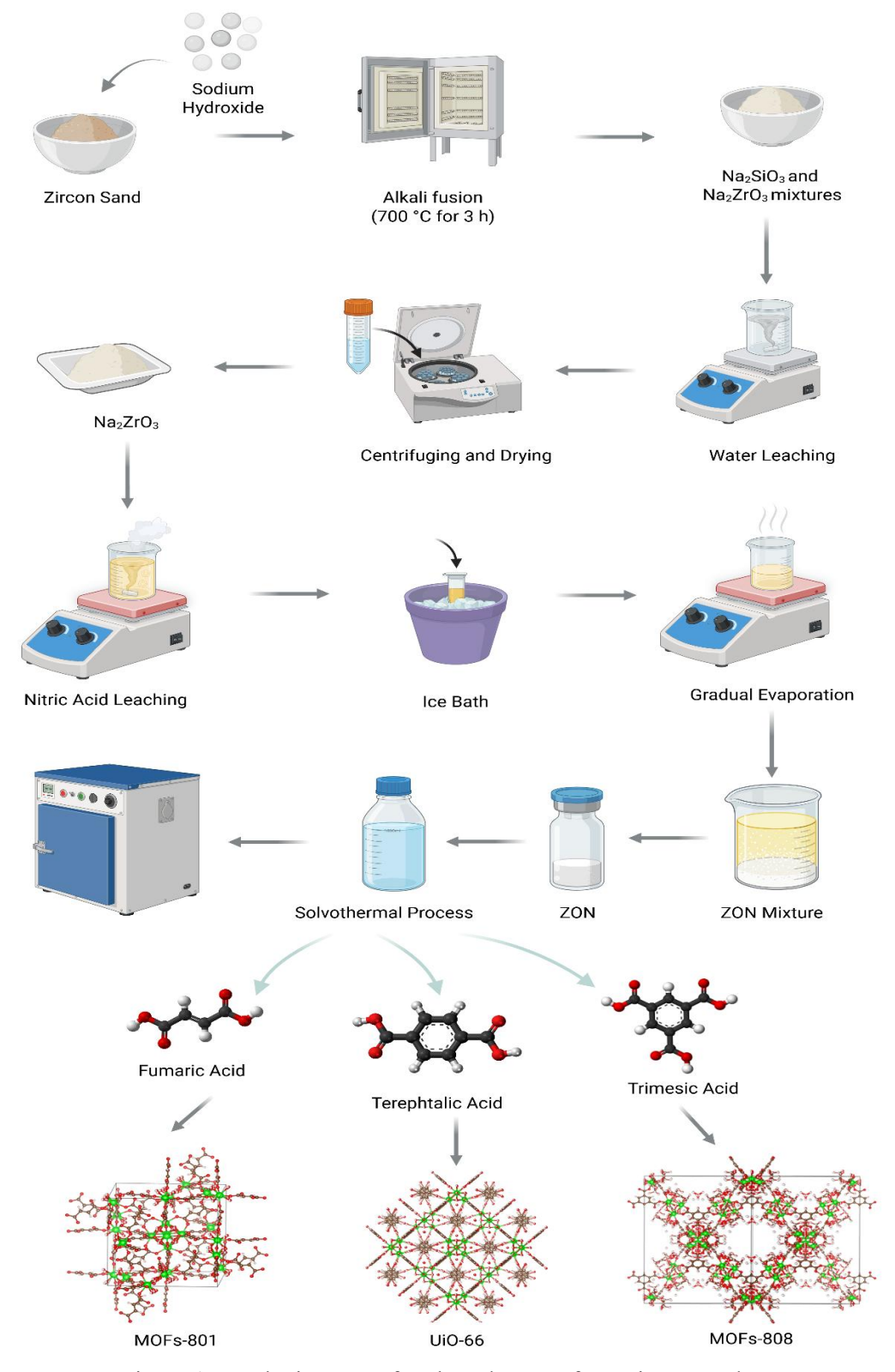


Figure 1. Synthetic route of Zr-based MOFs from zircon sand

RESULTS AND DISCUSSION

ZON Properties

The leaching process of zircon sand involves three main steps: alkali fusion, water leaching, and nitric acid leaching, resulting in the formation of the target product, zirconium nitrate species. Several stoichiometric reactions occurring throughout these stages are outlined below.

1. Alkali Fusion

During this step, the Zr–O–Si bonds in zircon mineral (ZrSiO₄) are broken by alkaline reagents at elevated temperatures, yielding sodium zirconate and sodium silicate species. The overall reaction proceeds as follows:

$$ZrSiO_{4(s)} + 4NaOH_{(l)} \rightarrow Na_2SiO_{3(s)} + Na_2ZrO_{3(s)} + 2H_2O_{(g)}$$

2. Water Leaching

In this stage, sodium silicate dissolves in water and undergoes hydrolysis, whereas sodium zirconate remains insoluble and is retained in the solid phase during washing. Further polymerization of the silicate species is confirmed by the formation of a white colloidal precipitate, observed as a residue during washing (Scott et al. 2024). This process is accompanied by a gradual decrease in solution pH, resulting from the dilution and removal of residual alkaline components from the alkali fusion step.

$$\begin{split} Na_2 SiO_{3(s)} + & H_2O_{(l)} \rightarrow Na^+_{(aq)} + SiO_3^{2^-}_{(aq)} \\ SiO_3^{2^-}_{(aq)} + & H_2O_{(l)} \iff HSiO_3^-_{(aq)} + OH^-_{(aq)} \\ SiO_3^{2^-}_{(aq)} + & H_2O_{(l)} \iff H_2SiO_{3(aq)} + OH^-_{(aq)} \\ & nH_2SiO_{3(aq)} \rightarrow (SiO_2)_n.xH_2O_{(s)} \end{split}$$

3. Nitric Acid Leaching

In this stage, sodium zirconate (Na₂ZrO₃) dissolves and reacts with nitric acid, releasing Zr⁴⁺ ions into the solution. As a highly oxophilic cation, Zr⁴⁺ readily undergoes hydrolysis in aqueous media; therefore, the solution pH is maintained below 2 to minimize the extent of hydrolysis. Under these acidic conditions, hydroxide species partially formed without complete precipitation as Zr(OH)₄ (Ma, et al. 2020; Abdullah et al. 2021). The resulting Zr(OH)₂²⁺ species coordinates with two nitrate ions (NO₃⁻) from nitric acid, forming a zirconium nitrate complex that precipitates as a hydrated crystalline salt.

 $Na_2ZrO_{3(s)} + 4HNO_{3(aq)} \rightarrow Zr(OH)_2(NO_3)_2 \cdot xH_2O_{(s)} + 2NaNO_{3(aq)}$

The composition, functional groups, structure, and morphology of the synthesized ZON were

characterized using XRF, FTIR, XRD, and SEM-EDX techniques. XRF analysis revealed that the natural zircon sand contained a relatively high zirconium content (73.554%), along with silica (24.313%), hafnium (1.520%), and several minor elements, as summarized in Table 1.

Table 1. XRF results of zircon sand, after alkali

| fusion and washing, and ZON | | | |
|-----------------------------|---------|------------|--------|
| Elements | %Wt | %Wt | %Wt |
| | (Zircon | (Zircon | (ZON) |
| | Sand) | Sand After | |
| | | Alkali | |
| | | Fusion and | |
| | | Washing) | |
| Si | 24.313 | 8.176 | 2.935 |
| Ca | 0.177 | 0.4480 | 0.220 |
| Ti | 0.062 | 0.111 | 0.083 |
| V | 0.003 | 0.012 | 0.010 |
| Mn | 0.069 | 0.028 | 0.037 |
| Fe | 0.303 | 0.119 | 0.112 |
| Hf | 1.520 | 1.731 | 1.730 |
| Zr | 73.554 | 89.375 | 94.873 |

Compared to previous studies (Dahlan et al., 2010; Saleh and Pramasanto, 2012), the mineral content of zircon sand from Kalimantan exhibits significant variation, likely due to differing geographical and geological conditions across regions. The alkali fusion process, followed by sequential leaching with water and nitric acid, resulted in a substantial enrichment of zirconium in the ZON sample, reaching 94.873%. The current approach utilizes only half of the conventional processing steps, eliminating the need for precipitation using sulfate bases and subsequent leaching with acid (Amliliana & Muzakky, 2021). This simplified process offers clear advantages in terms of time and cost efficiency, while still yielding a highly concentrated zirconium product. As shown in Figure 2a, FTIR analysis further supports the successful transformation of the material during the synthesis process. The spectrum of raw zircon sand displays characteristic absorption bands corresponding to Si-O stretching at 1003 cm⁻¹ (Sekewael et al. 2018; Sekewael 2021; Kiat et al. 2024) and Zr-O vibrations at 602 cm⁻¹ (Hani et al. 2023; Hasanien et al., 2024). Following alkali fusion and washing, the Si-O absorption band decreases in intensity and shifts in position, indicating the breakdown of the silicate framework and the increasing dominance of Zr-O bonding. In the ZON sample, the Si-O band is no longer observed, and new absorption bands emerge in the 527-800 cm⁻¹ region, which are attributed to Zr-O-Zr vibrational modes. An

additional band at 1384 cm⁻¹ indicates the presence of nitrate ions (NO₃⁻).

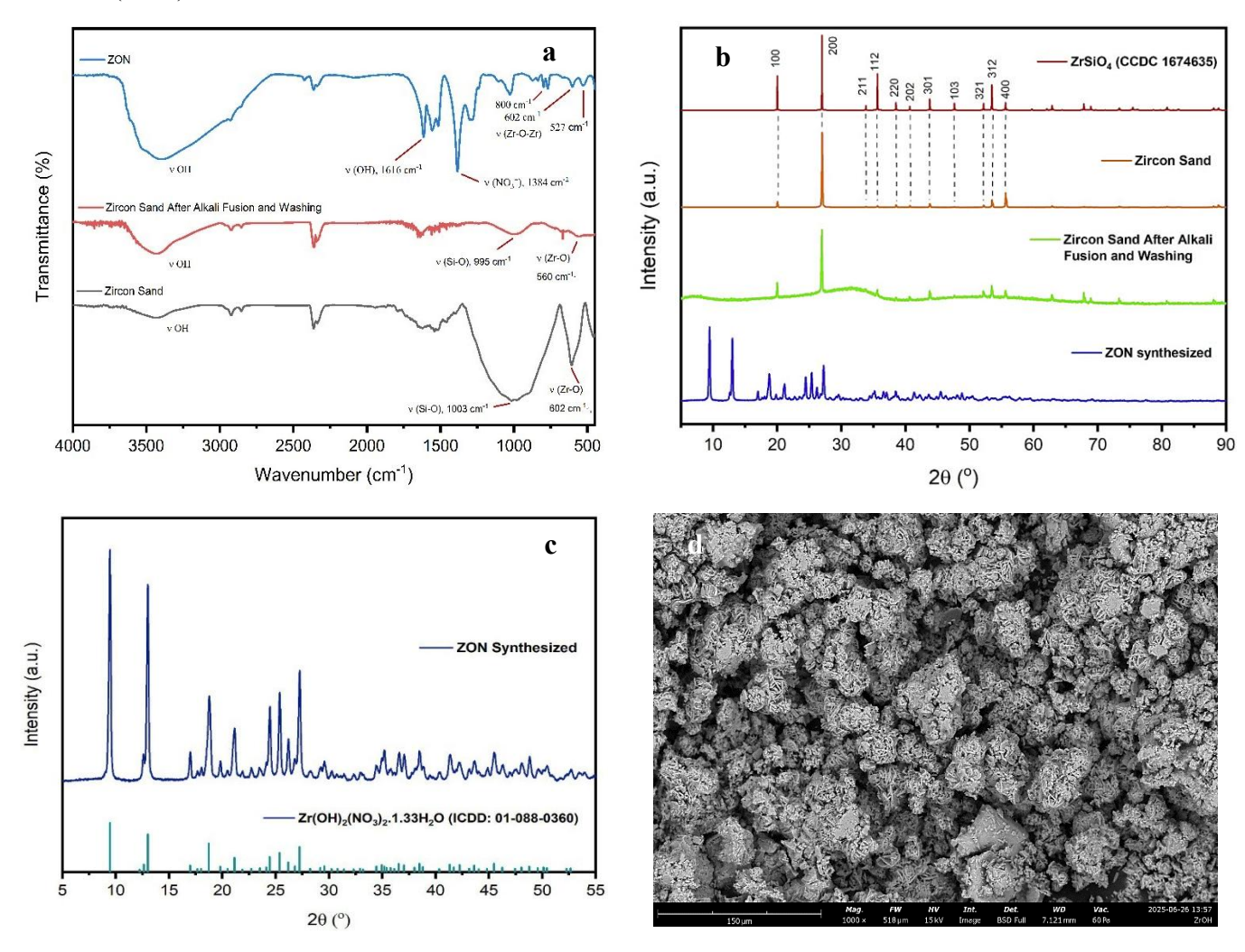


Figure 2. (a) FTIR spectra and (b) XRD patterns of zircon sand and its leaching products; (c) XRD pattern and (d) SEM image of the synthesized ZON.

A strong O-H absorption band at 1616 cm⁻¹ further suggests the presence of hydroxyl groups, likely originating from coordinated water molecules or hydroxide ligands within the complex. These results confirm that the ZON product is a novel zirconiumbased synthetic compound formed through structural transformation of zircon via alkali fusion followed by nitric acid leaching. XRD analysis (Figure 2b) revealed that the zircon sand exhibits sharp diffraction peaks that closely match the reference pattern for ZrSiO₄, indicating that the sample remains in a highly crystalline zircon mineral phase. Prominent peaks were observed at 2θ values of 20.01° (100), 27.09° (200), 35.72° (112), 53.47° (312), and 55.64° (400). After undergoing alkali fusion and subsequent washing, the diffractogram shows a more amorphous character, as evidenced by peak broadening. This suggests partial

decomposition of the zircon crystal structure into an amorphous or semi-crystalline form, thereby enhancing the solubility of zirconium under acidic conditions. In contrast, the synthesized ZON sample displays a distinct diffraction pattern, different from the raw zircon sand and the intermediate leached product. The appearance of multiple sharp reflections in the low-angle region ($2\theta \approx 10-30^{\circ}$) indicates the formation of a new crystalline synthetic phase. Previous studies have reported various zirconium nitrate compounds depending on synthesis pH and temperature, including ZrO(NO₃)₂, Zr(NO₃)₃(H₂O)₃⁺, (NO₂)[Zr(NO₃)₃(H₂O)₃]₂(NO₃) (Morozov et al. 2005), Zr(OH)₂(NO₃)₂·4.7H₂O (Bénard, Louër, & Louër, 1991). The XRD pattern of the synthesized ZON sample, when compared to the ICDD reference database (PDF No. 01-088-0360), confirms the

formation of Zr(OH)₂(NO₃)₂·1.33H₂O, as shown in Figure 2c. These findings suggest that the compound is formed under reaction conditions that precipitation of a hydrated phase and partial hydroxylation of zirconium species. Under highly acidic conditions (pH < 1), the excess of NO₃⁻ ions may transiently stabilize Zr4+ through the formation of Zr(NO₃)₄ species. However, this complex is highly unstable and prone to hygroscopicity upon exposure to air. Therefore, precise pH control is critical to ensure the formation of more stable zirconium species that are suitable as precursors for MOFs synthesis. The use of Zr(OH)₂(NO₃)₂·1.33H₂O as a zirconium precursor is particularly noteworthy, as no prior reports have documented its application as a starting metal source in synthesizing Zr-based MOFs. SEM micrographs of the synthesized ZON material reveal an aggregated morphology with a cabbage-like ablative structure, as shown in Figure 2d.

MOFs Properties

The synthesis of zirconium-based metal-organic frameworks (Zr-MOFs) generally proceeds via three fundamental steps: (i) hydrolysis of Zr4+ ions, (ii) formation of zirconium oxo-clusters, and (iii) coordination with organic linkers to construct the three-dimensional MOF framework. The presence of hydroxyl groups in the precursor Zr(OH)₂(NO₃)₂·1.33H₂O facilitates both hydrolysis and subsequent condensation processes, particularly through the formation of μ-O (bridging oxo) centers in the Zr₆O₄ cluster, which requires the condensation of at least two hydroxyl groups. This pathway promotes the rapid generation of the cationic hexanuclear cluster Zr₆O₄(OH)₄¹²⁺. This cluster subsequently coordinates with protonated organic linkers (in DMF), forming various Zr-MOFs.

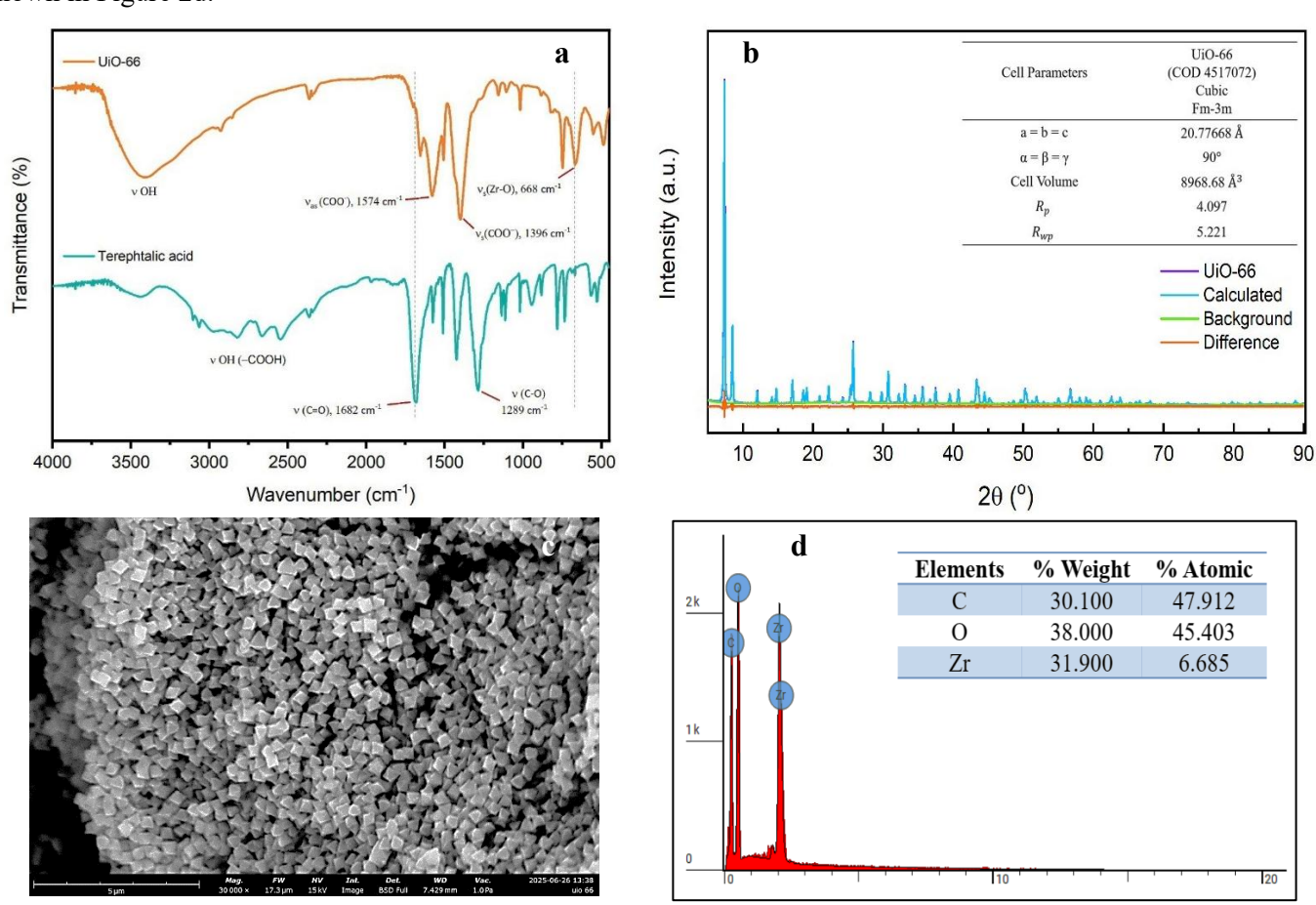


Figure 3. (a) FTIR spectra and (b) XRD patterns (c) SEM image d) EDX spectra of the synthesized UiO-66

FTIR analysis confirmed the successful synthesis of UiO-66 (Figure 3a). The absorption bands at 1574 and 1396 cm⁻¹ are attributed to the asymmetric and symmetric stretching vibrations of carboxylate (COO⁻) groups from terephthalic acid, indicating deprotonation and coordination to Zr nodes. A distinct band at 668 cm⁻¹ corresponds to the Zr–O stretching vibration, confirming the formation of coordination bonds between Zr and oxygen in the Zr₆O₄(OH)₄ cluster. This is further supported by a narrowing of the O–H stretching band, associated with hydroxyl groups in the cluster. The powder X-ray diffraction pattern

(Figure 3b) exhibits characteristic reflections at $2\theta = 7.38^{\circ}$ (111), 8.52° (200), and 25.72° (442), which match well with the simulated pattern (COD 4512072). Le Bail refinement indicates that the synthesized UiO-66 crystallizes in the cubic phase with space group Fm-3m. The refined unit cell parameters are shown in Figure 3b. SEM images (Figure 3c) show a homogeneous octahedral morphology, consistent with literature reports (Zhao et al. 2013; Miyamoto et al. 2015). EDX analysis (Figure 3d) confirms the presence of major elements C, O, and Zr in the synthesized UiO-66 framework .

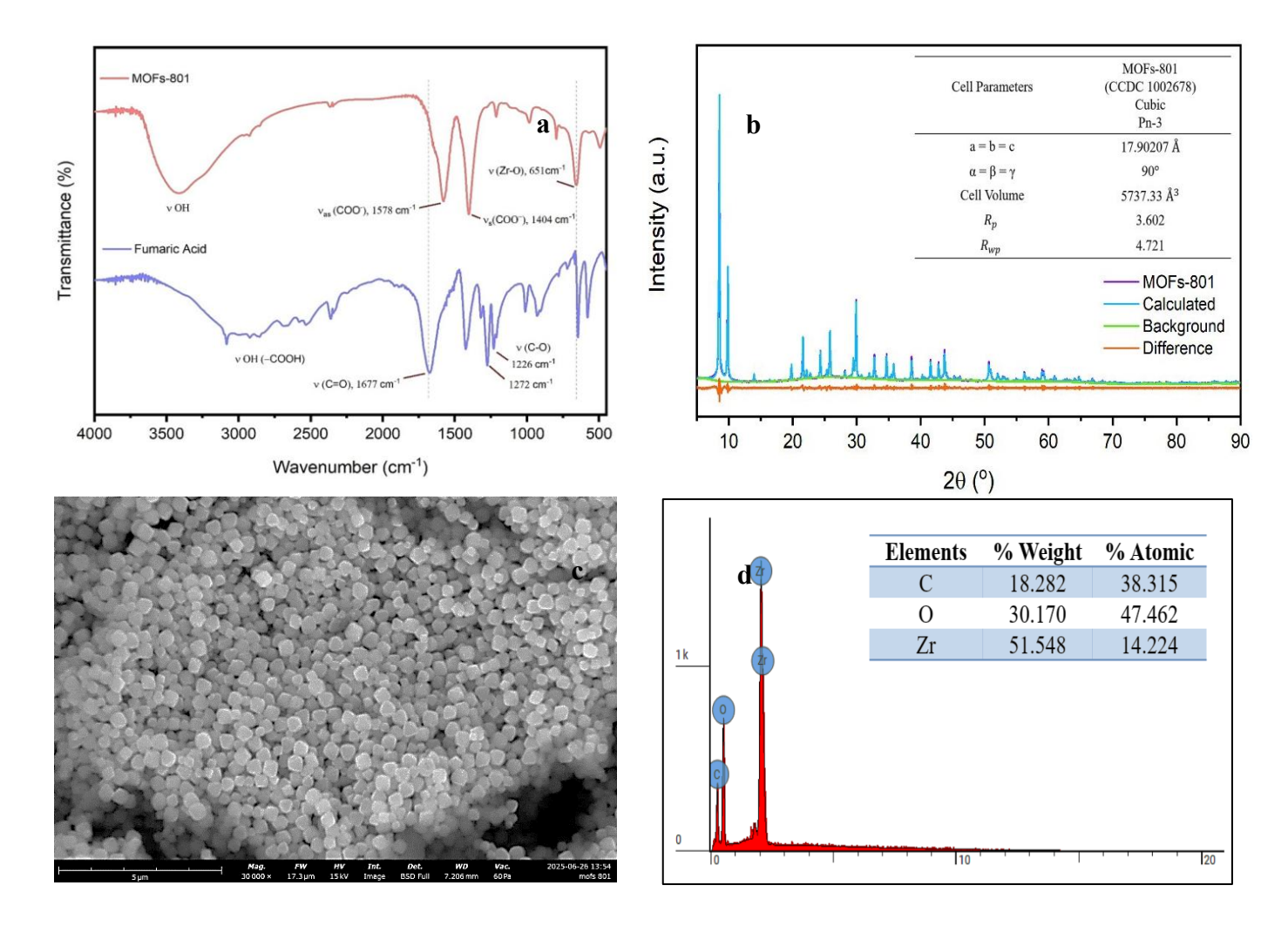


Figure 4. (a) FTIR spectra and; (b) XRD patterns; (c) SEM image; d) EDX spectra of the synthesized MOFs-801

FTIR analysis (Figure 4a) confirms the successful synthesis of the MOF-801 material. The disappearance of the carbonyl stretching vibration v(C=O) at 1677 cm⁻¹, replaced by two prominent bands at 1578 cm⁻¹ and 1404 cm⁻¹, corresponding to the asymmetric and symmetric stretching vibrations of coordinated carboxvlate groups (COO⁻), indicates that the –COOH groups have undergone deprotonation and are now involved in coordination with Zr4+ centers. This shift provides evidence of coordination bond formation between the oxygen atoms of the carboxylate ligands and the zirconium metal centers. Additionally, the emergence of a new absorption band at 651 cm⁻¹, associated with the stretching vibration of Zr-O bonds, suggests the binding of carboxylate groups to zirconium clusters within the MOFs structure. The broad and weakened O-H stretching band observed at higher wavenumbers (~3400 cm⁻¹) is attributed to

coordinated hydroxyl groups or residual water molecules residing in the MOFs pores. The X-ray diffraction pattern of the synthesized MOF-801 (Figure 4b) displays characteristic peaks at 2θ values that match well with the simulated pattern (CCDC 1002678), including distinct reflections at 8.53° (111), 9.84° (200), and 29.89° (442). Le Bail refinement confirms that the synthesized MOF-801 crystallizes in a cubic phase with space group Pn-3. The refined unit cell parameters are shown in Figure 4b. SEM micrographs of the synthesized MOF-801 (Figure 4c) reveal uniformly distributed, crystalline particles with well-defined faceted surfaces. The particles exhibit near-octahedral or polyhedral morphology, a typical feature of the cubic topology of MOF-801, constructed from Zr₆O₄(OH)₄ clusters and fumaric acid linkers (Jahan et al. 2022). EDX analysis (Figure 4d) indicates that the synthesized UiO-66 contains three major elements: carbon (C), oxygen (O), and zirconium (Zr)

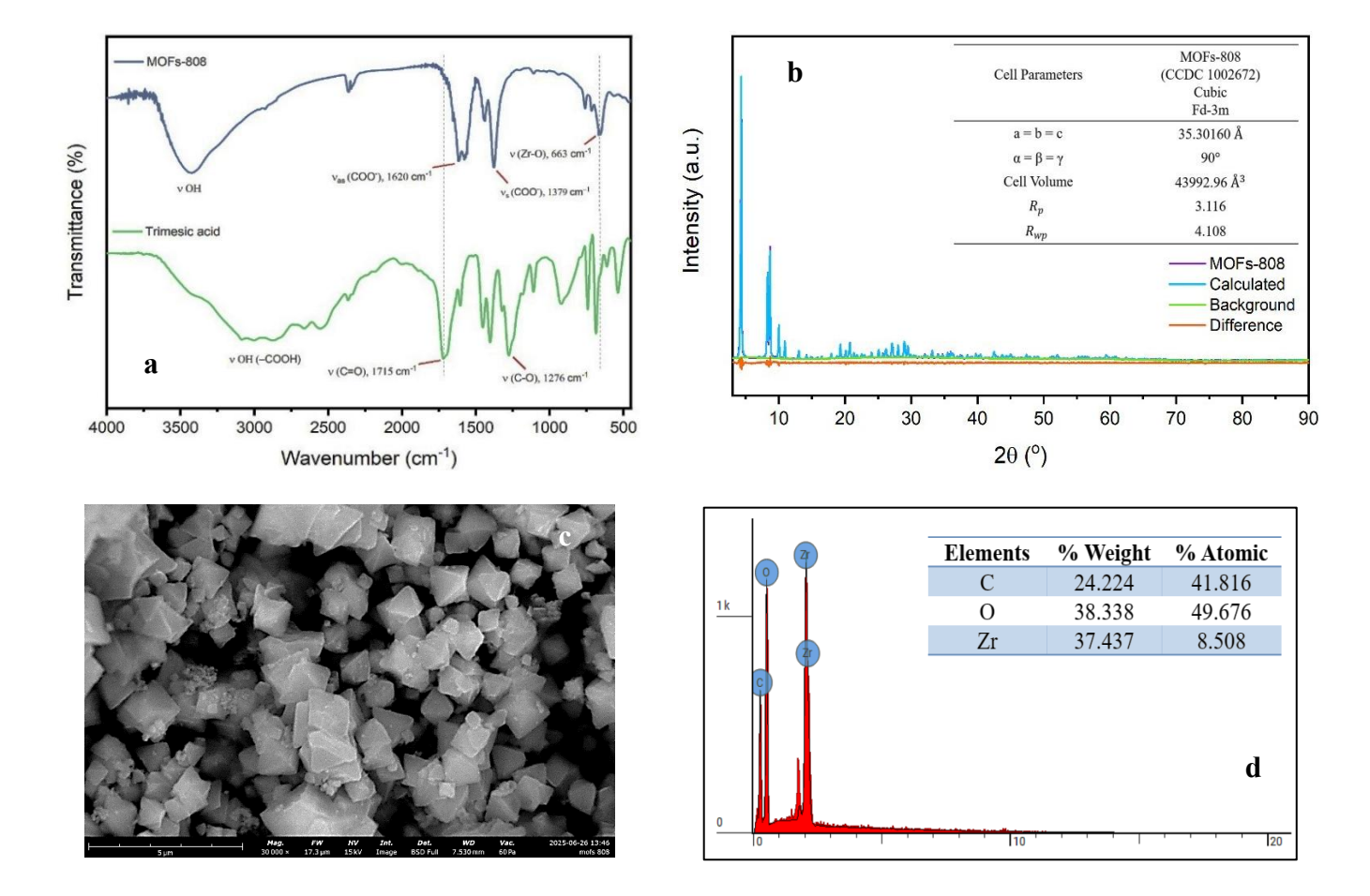


Figure 5. (a) FTIR spectra and (b) XRD patterns (c) SEM image d) EDX spectra of the synthesized MOFs-808

The FTIR spectrum (Figure 5a) of trimesic acid (H₃BTC) exhibits a sharp absorption band at 1715 cm⁻¹, corresponding to the C=O stretching vibration of free carboxylic acid groups, along with a band at 1276 cm⁻¹ attributed to C-O stretching. A broad O-H stretching band in the 3000-3500 cm⁻¹ region further confirms the presence of uncoordinated carboxylic acid functionalities. In contrast, the spectrum of the synthesized MOFs-808 reveals significant shifts indicative of successful coordination between the carboxylate ligands and Zr⁴⁺ centers. The disappearance of the C=O band at 1715 cm⁻¹, together with the emergence of asymmetric (v_{as} COO⁻) and symmetric (v_s COO⁻) carboxylate stretching bands at 1620 and 1379 cm⁻¹, respectively, confirms the deprotonation of the carboxylic acid groups and their coordination to zirconium nodes. Moreover, a new absorption band at 663 cm⁻¹, assigned to Zr-O vibrations, supports the formation of Zr-oxo clusters within the MOF framework. The broad O-H band observed in the MOFs-808 spectrum is likely due to residual water molecules or coordinated hydroxyl groups. These spectral features collectively confirm the successful formation of MOFs-808 through coordination-driven self-assembly of trimesic acid with zirconium clusters. The powder X-ray diffraction pattern (Figure 5b) of the synthesized MOFs-808 exhibits characteristic reflections consistent with the simulated data (CCDC 1002672), with prominent peaks observed at $2\theta = 4.34^{\circ}$ (111), 8.30° (311), and 8.68° (222). Le Bail refinement confirms that the synthesized material crystallizes in a cubic phase with space group Fd-3m. The refined unit cell parameters are summarized in Figure 5b. Scanning electron microscopy (Figure 5c) reveals that the MOFs-808 particles possess a uniform crystalline morphology, predominantly octahedral in shape, which is typical of Zr-MOFs (Li et al. 2015). Energy-dispersive X-ray spectroscopy (Figure 5d) analysis confirms the presence of three major elements C, O, and Zr in the synthesized MOFs-808.

CONCLUSION

This study successfully demonstrated the transformation of natural zircon sand into a zirconium nitrate hydrate compound (ZON), which proved to be an effective precursor for synthesizing Zr-MOFs. Through an efficient three-step leaching process, a zirconium content of 94.87% was achieved, highlighting the effectiveness of nitric acid as a leaching agent. The ZON compound was shown to undergo hydrolysis and condensation processes, which are crucial for forming the $Zr_6O_4(OH)_4$ cluster core.

Three MOF materials, UiO-66, MOFs-801, and MOFs-808 were successfully synthesized via solvothermal methods, exhibiting structural and morphological characteristics consistent with those reported in the literature. These results indicate that local zircon sand is not only viable as an alternative zirconium source but also valuable for developing high-value functional materials. By introducing ZON as a novel precursor in MOFs synthesis, this study offers a more environmentally friendly and cost-effective approach to the development of functional materials, while also reinforcing the sustainable utilization of local mineral resources.

ACKNOWLEDGMENT

The authors would like to acknowledge Politeknik STTT Bandung for providing access to the SEM-EDX facilities used in this study. BVP gratefully acknowledges the support of the Lembaga Pengelola Dana Pendidikan (LPDP), Ministry of Finance of the Republic of Indonesia, for funding his master's program and supporting the completion of this journal.

REFERENCES

- Abdullah, M., Triwikantoro, T., Umamah, C., & Andi, H. J. (2021). The effect of pH and calcination temperature on the ZrO₂ phase formation from natural zircon sand of kereng pangi. *Jurnal Neutrino*, *13*(2), 39–48.
- Ali, A. H. (2022). Production of highly purified zirconium oxide from zircon mineral leach liquor using bis-(2-ethylhexyl) phosphate as a promising extractant. *Chemical Papers*, 76(11), 6723–6734.
- Ali, Amr Hamdi, Abdo, S. M., & Dakroury, G. A. R. S. (2023). Zirconium preconcentration from zircon raffinate using gamma radiation—induced polymerization of reduced graphene oxide composite. *Environmental Science and Pollution Research*, 30(20), 58330–58345.
- Amliliana, R. A., & Muzakky, M. (2021). Synthesis of Low TENORM Zirconium Sulfate from ZrO(OH)₂ with Sulfuric Acid. *Indonesian Journal of Chemistry*, 21(4), 842.
- Bénard, P., Louër, M., & Louër, D. (1991). Crystal structure determination of Zr(OH)₂(NO₃)₂· 4.7H₂O from X-ray powder diffraction data. *Journal of Solid State Chemistry*, 94(1), 27–35.
- Chattopadhyay, K., Mandal, M., & Maiti, D. K. (2024). A review on zirconium-based metal-organic

- frameworks: Synthetic approaches and biomedical applications. *Materials Advances*, 5(1), 51–67.
- Da Silva, R. J. F., Dutra, A. J. B., & Afonso, J. C. (2012). Alkali fusion followed by a two-step leaching of a Brazilian zircon concentrate. *Hydrometallurgy*, 117–118, 93–100.
- Ebrahim, A., Ghali, M., & El-Moneim, A. A. (2024). Microporous Zr-metal-organic frameworks based-nanocomposites for thermoelectric applications. *Scientific Reports*, *14*(1), 13067.
- Emsley, J. (2014). In Your Element: The A–Z of zirconium. *Nature Chemistry*, 6(11), 1026–1026
- Finch, R. J. (2003). Structure and Chemistry of Zircon and Zircon-Group Minerals. *Reviews in Mineralogy and Geochemistry*, 53(1), 1–25.
- Gutiérrez-Serpa, A., Pasán, J., Jiménez-Abizanda, A. I., Kaskel, S., Senkovska, I., & Pino, V. (2022). Thin-film microextraction using the metal-organic framework DUT-52 for determining endocrine disrupting chemicals in cosmetics. *Microchemical Journal*, 181, 107685.
- Hani, A., Meftah, N., Zeghoud, L., Sdiri, A., & Jawad, A. H. (2023). Statistical Optimization and Desirability Function for Producing Nano Silica from Dune Sand by Sol–gel Method Towards Methylene Blue Dye Removal. *Journal of Inorganic and Organometallic Polymers and Materials*, 33(7), 1882–1897.
- Hasanien, Y. A., Mosleh, M. A., Abdel-Razek, A. S., El-Sayyad, G. S., El-Hakim, E. H., & Borai, E. H. (2024). Green synthesis of SiO2 nanoparticles from Egyptian white sand using submerged and solid-state culture of fungi. *Biomass Conversion and Biorefinery*, *14*(20), 26159–26172. https://doi.org/10.1007/s13399-023-04586-y
- Jahan, I., Rupam, T. H., Palash, M., Rocky, K. A., & Saha, B. B. (2022). Energy efficient green synthesized MOF-801 for adsorption cooling applications. *Journal of Molecular Liquids*, 345, 117760.
- Kiat, J., Bijang, C. M., Sutapa, W., & Sekewael, S. J. (2024). Synthesis And Characterization Of Silver Nanoparticles Using Gandaria (Bouea macrophylla Griff.) Seed Extract As Bioreductor And Ouw Natural Clay (ONC) As Matrix. *Indo J Chem Res*, 12(2), 164–172.
- Li, Z.-Q., Yang, J.-C., Sui, K.-W., & Yin, N. (2015). Facile synthesis of metal-organic framework

- MOF-808 for arsenic removal. *Materials Letters*, 160, 412–414.
- Lv, D., Xu, J., Zhou, P., Tu, S., Xu, F., Yan, J., Xia, Q. (2022). Highly selective separation of propylene/propane mixture on cost-effectively four-carbon linkers based metal-organic frameworks. *Chinese Journal of Chemical Engineering*, 51, 126–134.
- Ma, Y., Stopic, S., Wang, X., Forsberg, K., & Friedrich, B. (2020). Basic Sulfate Precipitation of Zirconium from Sulfuric Acid Leach Solution. *Metals*, 10(8), 1099.
- Miyamoto, M., Kohmura, S., Iwatsuka, H., Oumi, Y., & Uemiya, S. (2015). In situ solvothermal growth of highly oriented Zr-based metal organic framework UiO-66 film with monocrystalline layer. *CrystEngComm*, 17(18), 3422–3425.
- Morozov, I. V., Fedorova, A. A., Palamarchuk, D. V., & Troyanov, S. I. (2005). Synthesis and crystal structures of zirconium(IV) nitrate complexes (NO₂)[Zr(NO₃)₃(H₂O)₃]₂(NO₃)₃,Cs[Zr(NO₃)₅], and (NH₄)[Zr(NO₃)₅](HNO₃). Russian Chemical Bulletin, 54(1), 93–98.
- Nadliriyah, N., Putri, A. L., & Triwikantoro, T. (2019). PANi/ZrO₂ -composite coating for corrosion protection in 3.5 M NaCl solution. *IOP Conference Series: Materials Science and Engineering*, 496, 012059.
- Nguyen, K. D., Ho, P. H., Vu, P. D., Pham, T. L. D., Trens, P., Di Renzo, F., Le, H. V. (2021). Efficient Removal of Chromium(VI) Anionic Species and Dye Anions from Water Using MOF-808 Materials Synthesized with the Assistance of Formic Acid. *Nanomaterials*, 11(6), 1398.
- Nguyen, K. D., Vo, N. T., Le, K. T. M., Ho, K. V., Phan, N. T. S., Ho, P. H., & Le, H. V. (2023). Defect-engineered metal-organic frameworks (MOF-808) towards the improved adsorptive removal of organic dyes and chromium (VI) species from water. *New Journal of Chemistry*, 47(13),6433-6447.
- Permadani, I., Phasa, D. A., Pratiwi, A. W., & Rahmawati, F. (2016). The Composite of ZrO₂-TiO₂ Produced from Local Zircon Sand Used as A Photocatalyst for The Degradation of Methylene Blue in A Single Batik Dye Wastewater. *Bulletin of Chemical Reaction Engineering & Catalysis*, 11(2), 133–139.
- Qiu, J., Feng, Y., Zhang, X., Jia, M., & Yao, J. (2017). Acid-promoted synthesis of UiO-66 for highly selective adsorption of anionic dyes:

- Adsorption performance and mechanisms. *Journal of Colloid and Interface Science*, 499, 151–158.
- Rahmawati, F., Permadani, I., Heraldy, E., Syarif, D. G., & Soepriyanto, S. (2016). Structure and morphological analysis of various composition of yttrium doped-zirconia prepared from local zircon sand. *Journal of Physics: Conference Series*, 776, 012050.
- Ru, J., Wang, X., Wang, F., Cui, X., Du, X., & Lu, X. (2021). UiO series of metal-organic frameworks composites as advanced sorbents for the removal of heavy metal ions: Synthesis, applications and adsorption mechanism. *Ecotoxicology and Environmental Safety*, 208, 111577.
- Sajima, Handini, T., Suyanti, & Sudaryadi. (2020). Separation the zircon mineral from tailing Tin mining using shaking table. *Journal of Physics: Conference Series*, 1436(1), 012127.
- Sekewael, S. J., Wijaya, K., & Triyono. (2018). Pengaruh pemanasan terhadap kristalinitas dan parameter kisi nanokomposit Silika-Zirkonia montmorillonit K10 dan Silika-Besi oksida montmorillonit K10. *Indo J Chem Res*, *6*(1), 38–43.
- Sekewael, S. J. (2021). Determination of surface acidity on the natural and synthetic montmorillonite clays by titration method. *Indo J Chem Res*, 9(2), 94–98.
- Scott, S., Galeczka, I. M., Gunnarsson, I., Arnórsson, S., & Stefánsson, A. (2024). Silica

- polymerization and nanocolloid nucleation and growth kinetics in aqueous solutions. *Geochimica et Cosmochimica Acta*, 371, 78–94
- Su, H., Lv, S., Song, H., Shi, K., Zhu, J., & Zhang, Y. (2024). Recent advances in continuous zirconium-based metal-organic framework membranes for high-precision separation. Separation and Purification Technology, 345, 127318.
- Sun, Hongqian, Song, J., & Qi, T. (2024). Separation of Zr and Si in Zirconium Silicate by Sodium Hydroxide Sub-Molten Salt. *Metals*, 14(6), 630
- Sun, Hong-qian, Song, J., Sun, S., Qu, J., Lü, W., & Qi, T. (2019). Decomposition kinetics of zircon sand in NaOH sub-molten salt solution. Transactions of Nonferrous Metals Society of China, 29(9), 1948–1955.
- Tahli, L., & Wahyudi, T. (2017). A characteristic study of popay zircon sand used for ceramics, refractory and foundry raw materials. *Indonesian Mining Journal*, 19(1), 1–17.
- Widayat, W., Almaas Salwa, D. A., Hasanah, A., Nisa, K., & Saudale, J. M. P. (2024). Preparation of Zirconia Catalyst from Zircon Sand and Catalytic Testing for Biodiesel Production. *Reaktor*, 24(2), 36–40.
- Zhao, Q., Yuan, W., Liang, J., & Li, J. (2013). Synthesis and hydrogen storage studies of metal-organic framework UiO-66. *International Journal of Hydrogen Energy*, 38(29), 13104–13109.